

Fourier-mode dynamics for the nonlinear Schrödinger equation in one-dimensional bounded domains

J. G. Caputo,^{1,*} N. K. Efremidis,^{2,†} and Chao Hang^{3,4,‡}

¹*Laboratoire de Mathématiques, INSA de Rouen, B. P.8, F-76801 Saint-Etienne du Rouvray, France*

²*Department of Applied Mathematics, University of Crete, GR-71409 Heraklion, Crete, Greece*

³*Centro de Física Teórica e Computacional, Faculdade de Ciências, Universidade de Lisboa, Avenida Professor Gama Pinto 2, Lisboa P-1649-003, Portugal*

⁴*Department of Physics and State Key Laboratory of Precision Spectroscopy, East China Normal University, Shanghai 200062, China*

(Received 31 March 2011; revised manuscript received 25 July 2011; published 12 September 2011)

We analyze the 1D focusing nonlinear Schrödinger equation in a finite interval with homogeneous Dirichlet or Neumann boundary conditions. There are two main dynamics, the collapse which is very fast and a slow cascade of Fourier modes. For the cubic nonlinearity the calculations show no long-term energy exchange between Fourier modes as opposed to higher nonlinearities. This slow dynamics is explained by fairly simple amplitude equations for the resonant Fourier modes. Their solutions are well behaved so filtering high frequencies prevents collapse. Finally, these equations elucidate the unique role of the zero mode for the Neumann boundary conditions.

DOI: [10.1103/PhysRevE.84.036601](https://doi.org/10.1103/PhysRevE.84.036601)

PACS number(s): 05.45.Yv, 42.65.Hw, 42.65.Wi

I. INTRODUCTION

The nonlinear Schrödinger equation in two or three spatial dimensions has been studied intensively, in particular because of the collapse phenomenon for the focusing case; see, for example, the reviews of Berge [1] and Sulem [2]. Most of these studies have been done for an infinite domain, for which the equation is invariant by a scaling transformation. This symmetry is important to determine the conditions for collapse. In many applications, like, for example, a laser propagating in an optical fiber, the domain is finite so the boundaries play an important role. In a finite domain with Dirichlet boundary conditions, Brezis and Gallouet [3] established the existence of a global solution for an initial condition whose L_2 norm is below threshold for the focusing case and in general for the defocusing case. With the same boundary conditions in \mathbb{R}^n , Strauss and Bu [4] established global existence for the defocusing case and a general power nonlinearity. A pioneering study was conducted by Fibich and Merle [5] for the 2D cubic nonlinear Schrödinger equation. They showed that circularly symmetric ground-state waveguide solutions are stable and that the critical power condition for collapse is sharp unlike for an infinite domain. For small amplitudes the ground states reduce to the Bessel linear modes of the Laplacian. An interesting problem is then how these modes exchange energy as the solution evolves. This issue is important since some of these modes can be filtered out.

More generally, the energy exchange between linear modes is related to the old problem studied by Fermi-Pasta and Ulam (see the first section of Ref. [6] for subsequent developments). For a chain of oscillators with cubic nonlinearities, a medium-amplitude Fourier mode initial condition gives rise to a cascade of higher Fourier modes and energy flows back into the initial mode. For the focusing cubic nonlinear Schrödinger equation in 1D we expect a similar recurrence because of the

integrability of the model on the infinite line. Here the solution evolves into pulses due to the modulational instability. The dynamics of these solitons in domains with Dirichlet, Neumann, or Robin boundary conditions was studied numerically by Ramos and Villatoro [7], who validated a formalism based on images. For periodic boundary conditions, the dynamics of an isolated pulse is close to linear since the Fourier modes are weakly coupled as shown by Erdogan and Zharnitsky [8]. This dynamics differ from what happens in turbulence where there is a one-way flow of energy in wave numbers. For example, Muraki [9] studied this one-way cascade for the Burgers equation. Using the Cole-Hopf transformation, he was able to quantify the phenomenon. Finally, note the study [10] by Zakharov, Dias, and Pushkarev of wave turbulence carried out on a 1D model in Fourier space.

Following a similar approach, in this article we have analyzed the 1D nonlinear Schrödinger equation with cubic and quintic nonlinearities on a finite interval with Dirichlet or Neumann boundary conditions. We have chosen to work in 1D to benefit from the Fourier machinery that enables to solve the problem numerically fairly easily. A relatively small number of Fourier modes are necessary to describe well the solution when it is not singular. Another advantage is that the analysis can be done easier than for the 2D case. We have studied the stationary solutions and their stability. We have also obtained simple models for the resonant transfer of energy between Fourier modes for the cubic and quintic nonlinearities. As expected, there is no resonant transfer for the cubic nonlinearity. For a quintic nonlinearity a resonant transfer exists. The solutions of these reduced models compare well to the numerical solutions of the partial differential equation. Their evolution is nonsingular, confirming that filtering prevents collapse. This method of analysis of the resonant transfers of energy can be extended to other operators or higher dimensions. The principle remains the same but, of course, the machinery will be much more complicated.

The article is organized as follows. In Sec. II we review the conservation laws and the virial identity, the main theoretical tool to establish fitness for both the Dirichlet and the Neumann

*caputo@insa-rouen.fr

†nefrem@tem.uoc.gr

‡chang@phy.ecnu.edu.cn

boundary conditions. Section III presents the ground states and their stability. Numerical results are shown in Sec. IV and explained in Sec. V by use of the model of resonant energy transfer. We conclude in Sec. VI.

II. CONSERVED QUANTITIES AND VIRIAL RELATIONS

We consider the one-dimensional nonlinear Schrödinger (NLS) equation

$$i\psi_t + \psi_{xx} + |\psi|^{2d}\psi = 0 \quad (1)$$

on the bounded domain $[0, \pi]$ with the homogeneous Dirichlet boundary condition

$$\psi(x=0) = \psi(x=\pi) = 0, \quad (2)$$

or the Neumann boundary condition

$$\psi_x(x=0) = \psi_x(x=\pi) = 0. \quad (3)$$

Here d is a positive integer with $d = 1, 2,$ and 3 corresponding to the cubic, quintic, and septic nonlinearities.

Equation (1) with both Dirichlet and Neumann boundary conditions admits the following conserved quantities, the L^2 norm

$$P = \int_0^\pi |\psi|^2 dx, \quad (4)$$

which is the total power in optics and the Hamiltonian

$$H = \int_0^\pi \left(|\psi_x|^2 - \frac{1}{d+1} |\psi|^{2d+2} \right) dx. \quad (5)$$

The momentum

$$\Pi = i \int_0^\pi (\psi \psi_x^* - \psi^* \psi_x) dx, \quad (6)$$

which is conserved for the infinite domain now has a flux

$$\Pi_t = -4[|\psi_x|^2]_0^\pi, \quad (7)$$

for Dirichlet boundary condition and

$$\Pi_t = \left[(|\psi|^2)_{xx} + \frac{2d}{d+1} |\psi|^{2d+2} \right]_0^\pi, \quad (8)$$

for Neumann boundary condition.

We can analyze the evolution of following integral quantities related with the model (1)

$$I_1(t) = \int_0^\pi |\psi|^2 x^2 dx, \quad (9a)$$

$$\begin{aligned} I_2(t) &= \int_0^\pi \left(|\psi_x|^2 - \frac{d}{2(d+1)} |\psi|^{2d+2} \right) dx \\ &= H - \frac{1}{2} \int_0^\pi \frac{d-2}{d+1} |\psi|^{2d+2} dx. \end{aligned} \quad (9b)$$

Here, I_1 is the variance, which is a common tool for predicting collapse of NLS equation solutions in infinite domain and we assume that I_j ($j = 1, 2$) are initially well defined.

For Dirichlet boundary, some algebra leads to

$$\frac{d^2 I_1}{dt^2} = -4\pi [|\psi_x|^2]_{x=\pi} + 8H - 4 \int_0^\pi \frac{d-2}{d+1} |\psi|^{2d+2} dx, \quad (10)$$

which shows that $H < 0$ is a sufficient condition for collapse. Note that the right-hand side of (10) can be negative even though $H > 0$. In the infinite domain the first term is absent. Therefore, compared with the infinite line, Dirichlet boundaries focus the solution and enhance the collapse.

For the Neumann boundary conditions, we have

$$\begin{aligned} \frac{d^2 I_1}{dt^2} &= 2\pi \left[(|\psi|^2)_{xx} + \frac{2d}{d+1} |\psi|^{2d+2} \right]_{x=\pi} \\ &\quad + 8H - 4 \int_0^\pi \frac{d-2}{d+1} |\psi|^{2d+2} dx. \end{aligned} \quad (11)$$

From Eq. (11) we note that $H < 0$ is not a sufficient condition for the collapse. Therefore, the Neumann boundary can be either reflecting or absorbing and enhance or suppress the collapse.

III. BOUND STATES

The time periodic solutions of Eq. (1) can be searched in the form

$$\psi(z, x) = u(x) \exp(iEt), \quad (12)$$

where $u(x)$ is a real function and E is the propagation constant that is also real. The resulting equation then reads

$$-Eu + u'' + u^{2d+1} = 0 \quad (13)$$

with the Dirichlet boundary conditions

$$u(x=0) = u(x=\pi) = 0 \quad (14)$$

and the Neumann boundary conditions

$$u_x(x=0) = u_x(x=\pi) = 0. \quad (15)$$

A conserved quantity of Eq. (13) can be found by multiplying with $u'(x)$ and integrating over x

$$K = \frac{1}{2} (u')^2 - \frac{E}{2} u^2 + \frac{1}{2d+2} u^{2d+2}, \quad (16)$$

which can be further integrated to give

$$\int dx = \pm \frac{1}{2} \int dz \left[z \left(4K + 2Ez - \frac{2}{d+1} z^{d+1} \right) \right]^{-1/2} \quad (17)$$

by defining $z = u^2$. The above integral can be expressed in terms of Jacobi elliptic functions in both the cases of cubic and quintic nonlinearities. However, in the latter case the resulting expressions are rather complicated.

The phase portrait associated with Eq. (16) is shown in Fig. 1 for $E = -1$ (left panel) and $E = 1$ (right panel). The points such that $u = 0$ ($u_x = 0$) correspond to the solutions boundaries for Dirichlet (Neumann) boundary conditions.

If $u \ll 1$, the nonlinearity does not play an important role and the solutions are close to the linear limit of Eq. (13), i.e.,

$$u_m(x) = A \sin(mx) \quad (18)$$

for the Dirichlet boundary condition and

$$u_m(x) = A \cos(mx) \quad (19)$$

for the Neumann boundary condition. Here m denotes the index of the wave number $m = 0, 1, 2, \dots$ and A denotes the

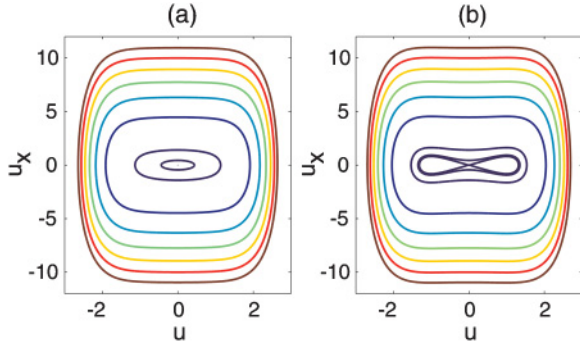


FIG. 1. (Color online) Phase portrait associated with Eq. (16) for $E = -1$ (a) and $E = 1$ (b) for $d = 2$. The levels presented for K are $K = 0, 0.1, 1, 10, 20, 30, 40, 50, 60$.

amplitude with $A \ll 1$. The propagation constant, K , and the power are then given by

$$E_m = -m^2, \quad K_m = \frac{m^2}{2}A^2, \quad P = \frac{\pi}{2}A^2. \quad (20)$$

When $|u|$ starts to increase, the propagation constant, as well as the form of the solutions, is slightly modified due to the effect of nonlinearity, i.e., $E = E_m + \delta E$ with $\delta E \ll E_m$. The relationship between the correction of the propagation constant δE and amplitude A (and thus P) can be computed by

$$\delta E = \frac{(2d+2)!}{2^{2d+1}[(d+1)!]^2} A^{2d} = \frac{(2d+2)!}{\pi^d 2^{d+1} [(d+1)!]^2} P^d. \quad (21)$$

When $u \sim 1$, the nonlinearity has a strong effect and we have to resort to numerical methods to find the solution. We also notice that Eq. (13) with the Neumann boundary condition admits constant solution, i.e., $u = A_0$ with $E = A_0^{2d} \geq 0$.

Figure 2 shows the solutions of Eq. (13) obtained via a shooting method for both Dirichlet and Neumann boundary conditions. The right panel shows the behavior $P(E)$. The stationary solutions $u(x)$ for $d = 2$ are shown. The initial conditions are the solutions of the linear problem (18) and (19). We see that the family of solutions with $m = 1$ bifurcates from zero at $E = E_1 = -1$ while the family of solutions with $m = 2$ bifurcates from zero at $E = E_2 = -4$. Close to the bifurcation points the $P - E$ curves follow the relation (21). $P(E)$ is monotonically increasing with the growth of E while $dP(E)/dE|_{E \rightarrow \infty} \rightarrow 0$.

The linear stability of the stationary solutions can be studied by solving numerically the linearized eigenvalue problem. Particularly, we assume that

$$\psi(x, t) = [u(x) + (\alpha + i\beta)]e^{iEt}, \quad (22)$$

where α, β are small perturbations that are proportional to $\exp(-i\lambda t)$. The coupled eigenvalue problem then reads

$$L_1 B = -i\lambda A, \quad L_2 A = i\lambda B, \quad (23)$$

where $L_1 = -\partial_{xx} + E - u(x)^{2d}$ and $L_2 = -\partial_{xx} + E - (2d+1)u(x)^{2d}$. The growth rate is defined as $\max[\text{Im}(\lambda)]$ at which an unstable solution will grow. We find that the family of solutions with $m = 1$ is always stable against linear perturbations, whereas only a very narrow stability region close to the bifurcation point exists for the family of solutions with $m = 2, 3, 4, \dots$

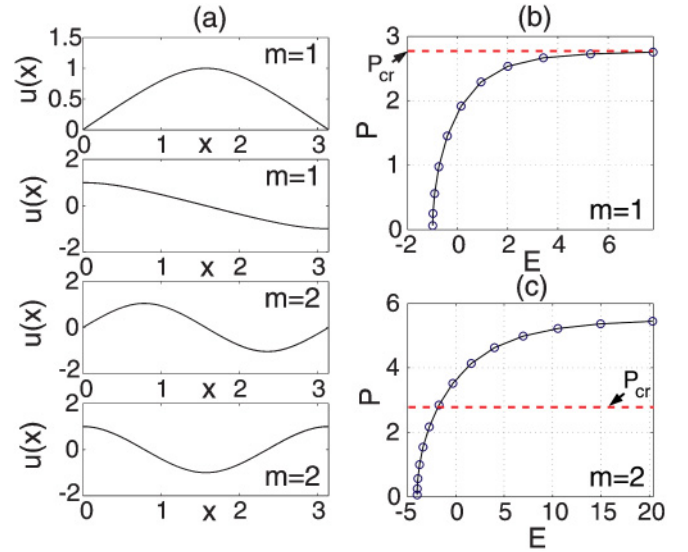


FIG. 2. (Color online) The stationary solutions $u(x)$ for $d = 2$. The initial conditions are taken as $\sin(mx)$ and $\cos(mx)$, naturally satisfying the Dirichlet and Neumann boundary conditions, respectively, with $m = 1$ [the upper two panels in (a)] and $m = 2$ [the lower two panels in (a)]. The dependence of P on E are shown in the (b) and (c) for $m = 1$ and $m = 2$, respectively. The total power $P|_{E \rightarrow \infty} \rightarrow 2.755$ for $m = 1$ and $P|_{E \rightarrow \infty} \rightarrow 5.447$ for $m = 2$. The dashed line (red online) denotes the value of P_{cr} from (25).

In the case of infinite domain, Eq. (13) admits the localized soliton solution

$$u = [(d+1)E]^{1/2d} \text{sech}^{1/d} \left[d\sqrt{E} \left(x - \frac{\pi}{2} \right) \right], \quad (24)$$

where the solution is centered in the center of the domain $x = \pi/2$. The total power for $d = 2$ is a constant

$$P_{\text{cr}} = \int |u|^2 dx = \frac{\pi}{4} \sqrt{12} = 2.72, \quad (25)$$

i.e., it is independent on E . The solutions with power $P < P_{\text{cr}}$ disperse during the propagation, whereas if $P > P_{\text{cr}}$ the solutions collapse. A similar analysis can be carried out for the case of $d = 3$ leading to

$$P_{\text{cr}} = \int |u|^2 dx = \frac{2^{5/3} \pi^{1/2} \Gamma(7/6)}{3^{1/2} \Gamma(2/3)} \frac{1}{E^{1/6}}, \quad (26)$$

which is expressed in terms of Γ functions and depends on E . Although the soliton solutions do not satisfy the NLS equation on a bounded domain with specific boundary conditions, they are particularly useful as limiting cases of solutions.

The solution (24) can be considered a good approximation to the solutions satisfying both Dirichlet and Neumann boundary conditions in the limit $E \rightarrow \infty$. This is because in this latter limit the maximum intensity increases as $E^{1/2}$ while the pulse width decreases as $E^{1/2}$. The narrowing of the pulse makes the soliton tails, as well as their derivatives, almost zero on the boundaries. The critical power for collapse P_{cl} does not change with the growth of E .

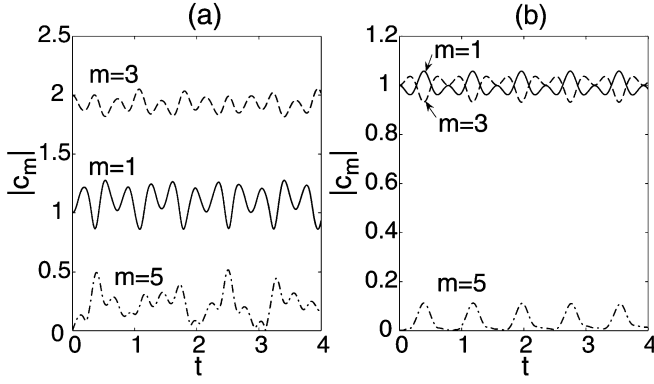


FIG. 3. Time evolution for a cubic nonlinearity and Dirichlet boundary conditions of the sine mode amplitudes $c_m(t), m = 1, 3, 5$ starting from two different initial conditions $\psi(0, x) = \sin(x) + 2 \sin(3x)$ shown in panel (a) and $\psi(0, x) = \sin(x) + \sin(3x)$ shown in panel (b).

IV. THE NUMERICAL SIMULATIONS

To understand the dynamics of the Fourier modes, we relied heavily on numerical solutions of the NLS equation on the interval $[0, \pi]$. As confirmed by the previous section, the well-posedness of the initial value problem is not trivial even for the quintic nonlinearity. We therefore concentrate our efforts on the cubic and quintic nonlinearities. For the latter and an initial condition close to collapse, we make sure that the solution remains regular by computing it on long time intervals.

The equation was solved using the split-step Fourier method where the linear part is advanced using the sine or cosine Fourier transforms, respectively, for Dirichlet and Neumann boundary conditions. Consider, for example, the Dirichlet boundary conditions. The sine Fourier modes form a complete and orthogonal set in $(0, \pi)$ so any function in $L^2(0, \pi)$ that satisfies Dirichlet boundary conditions can be expanded into these modes. The solution of the NLS has finite and constant L^2 norm and satisfies the boundary conditions. It can then be written as

$$\psi(t, x) = \sum_{m=1}^{\infty} c_m(t) \sin mx. \quad (27)$$

The details of the numerical implementation are given in the Appendix A.

We first describe the results for the Dirichlet boundary conditions. For $d = 1$, there is no collapse for Eq. (1). As expected, the evolution of a sine initial condition gives rise to a cascade of modes. For $c_1(0) = 2$ and $c_{j \neq 1}(0) = 0$ we observe a cascade to c_3 and c_5 with maximum amplitudes $\max(c_3) = 0.7$ and $\max(c_5) = 0.15$ with the other modes being insignificant. For $c_3(0) = 2$ and $c_{j \neq 3}(0) = 0$ we get almost no cascade.

Now let us compare the outcomes for $d = 1$ with the initial conditions $\psi(0, x) = \sin(x) + 2 \sin(3x)$ and $\psi(0, x) = \sin(x) + \sin(3x)$. The time evolution of the mode amplitudes are shown in Fig. 3. The mode amplitudes fluctuate in a fairly narrow range around an average value. This range decreases even more for smaller initial amplitudes as shown in the right panel. We will explain these effects in the next section.

Consider now the quintic case ($d = 2$) with Dirichlet boundary condition. In Fig. 4, we show the time evolution of

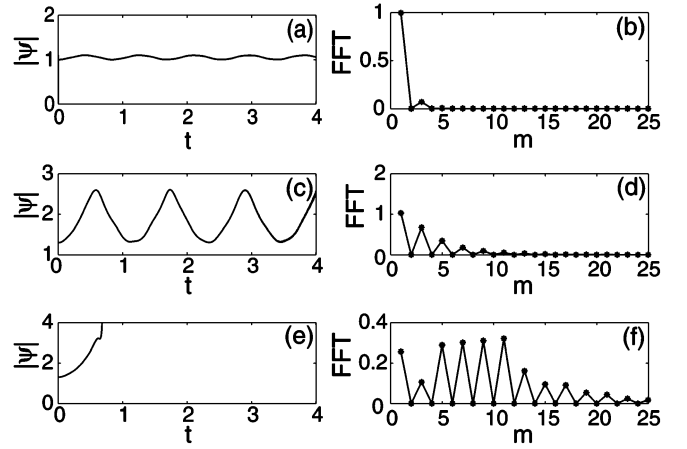


FIG. 4. [(a), (c), and (e)] Time evolution of the maximum of $|\psi|$ for a quintic nonlinearity and Dirichlet boundary conditions for three different initial conditions, from the top to the bottom, $\psi(0, x) = 1.0 \sin(x)$ ($P = 1.57$), $\psi(0, x) = 1.3 \sin(x)$ ($P = 2.65$), and $\psi(0, x) = 1.31 \sin(x)$ ($P = 2.70$). [(b), (d), and (f)] The corresponding Fourier spectra at time $t = 4$. Note the collapse occurring at $t \approx 0.7$ in the last row.

solution (18) with $m = 1$ and different values of amplitude A . No collapse is observed when $A(P)$ is small, whereas collapse occurs when $A > 1.3$ ($P > 2.65$). The condition $P > P_c$ for collapse seems to hold in this situation. A collapsing solution is shown on the last row of Fig. 4 for $A = 1.31$. The right panels of Fig. 4 show the Fourier spectra. We notice that only the odd modes are excited. Actually, we can explain that the cascade of Fourier modes for Eq. (1) starting with a particular mode q ($q = 0, 1, 2, \dots$) is always restricted to the modes $q(2n - 1)$ ($n = 1, 2, 3, \dots$) irrespective of the boundary conditions. In other words, we can expand the solutions of Eq. (1) as

$$\psi(t, x) = \sum_{n=1}^{\infty} c_{q(2n-1)} \sin[q(2n-1)x] \quad (28)$$

for the initial condition $\psi(0, x) = \sin(qx)$. For the Neumann boundary conditions the sines should be changed to cosines. Details are given in Appendix B. In Fig. 5, we show the recurrence of the solutions and spectrum cascade at different times when no collapse occurs. We will explain this phenomenon in the next section. We also note that for large propagation constant, the solutions appears in the form of the hyperbolic secant function.

In Fig. 6, we show the time evolution of the Fourier amplitudes for a initial condition (18) with $m = 1$ and increasing amplitude A . Each panel calculated for a single amplitude corresponds to different regions of similar behaviors for the modes. When $0 < A \leq 0.5$, there is only the mode $m = 1$. The other modes are insignificant. When $0.5 < A \leq 1.0$, we observe two modes $m = 1$ and 3 . When $1.0 < A \leq 1.2$, we observe three modes $m = 1, 3, 5$. When $1.2 < A \leq 1.3$, four modes, $m = 1, 3, 5$, and 7 , are observed. The larger the amplitude of the initial condition, the more modes are excited. When $A > 1.3$, collapse occurs. This is a much faster mechanism than the recurrence. The energy travels very suddenly from the low-frequency modes to the higher-frequency modes. For the Neumann boundary conditions, the

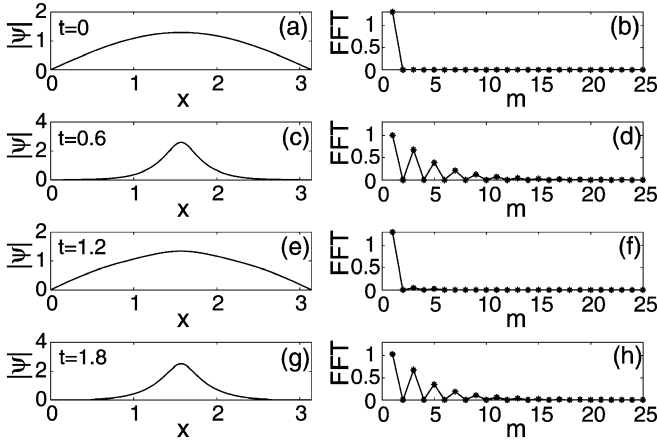


FIG. 5. Snapshots of the wave profiles [panels (a), (c), (e), and (g)] and corresponding Fourier spectra [(b), (d), (f), and (h)] for quintic nonlinearity and Dirichlet boundary condition. The times shown are $t = 0, 0.6, 1.2,$ and $1.8,$ respectively. The initial condition is $\psi(0) = 1.3 \sin(x)$ ($P = 2.65$). The recurrence of the wave profile and the spectrum cascade is evident. The profiles shown in (c) and (g) follow the hyperbolic secant function (24).

zero mode plays a special role. For example, it does not give rise to a spectrum cascade. We will see below how it couples to the other modes. Apart from this, the simulation results for the Neumann boundary conditions are similar to the ones for the Dirichlet boundary conditions.

V. EVOLUTION OF THE RESONANT FOURIER MODES

In the interval of existence of solutions, one can use the Fourier sine or cosine series depending on whether we have Dirichlet or Neumann boundary conditions. In both cases we have a complete basis for functions satisfying the boundary conditions. As opposed to the numerical method, here we require that at least the second derivative of the solution is continuous. Only then we can use the expansion to derive amplitude equations from the operator. We will first consider the Dirichlet boundary condition and examine cubic and

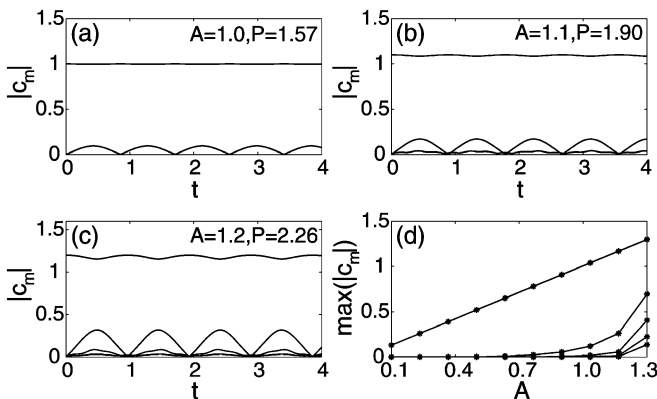


FIG. 6. Time evolution of the Fourier amplitudes for quintic nonlinearity and Dirichlet boundary condition for a 1 mode initial condition $c_1(0) = A = 1.0, 1.1,$ respectively, in panels (a), (b), and (c). Panel (d) shows $\max(|c_m|)$ for $m = 1, 3, 5, 7,$ and 9 as a function of the initial amplitude A .

quintic nonlinearities. The results that we will obtain for these are very similar for the Neumann boundary condition unless the zero mode is involved. This specific case will be addressed at the end of the section.

For the Dirichlet boundary conditions, we expand ψ in a sine Fourier series

$$\psi(x, t) = \sum_{m=1}^{\infty} c_m(t) \sin(mx), \quad (29)$$

where the c_m are given by

$$c_m(t) = \frac{2}{\pi} \int_0^{\pi} \psi(x, t) \sin(mx) dx. \quad (30)$$

Let us briefly discuss the collapse phenomenon. The conservation of the power implies for any m'

$$|c_{m'}(t)|^2 \leq \sum_{m=1}^{\infty} |c_m(t)|^2 = \frac{2}{\pi} P \equiv \mathcal{P}, \quad (31)$$

because of Parseval's relation,

$$\int_0^{\pi} |\psi|^2 dx = \frac{\pi}{2} \mathcal{P}.$$

When ψ is unbounded this relation still holds because the L_2 norm is conserved [11]. In that case the Fourier series converges to ψ in norm only and not pointwise. More precisely, when collapse occurs, it is in a given region of the interval $(0 : \pi)$. There the Fourier series ceases to converge pointwise to ψ . On the other hand, if ψ is continuous, the Fourier series converges to ψ uniformly and, of course, pointwise.

Substituting the expansion (29) into Eq. (1), we obtain the coupled equations of Fourier amplitudes. Note that we have assumed uniform convergence of the different Fourier series in order to invert the order of the sum and the integral. For the quintic nonlinearity ($d = 2$) we get

$$i\dot{c}_q - q^2 c_q + \frac{2}{\pi} \sum_{k,l,m,n,p} c_k c_l c_m c_n^* c_p^* \langle klmpq \rangle = 0, \quad (32)$$

where

$$\langle klmpq \rangle \equiv \int_0^{\pi} \sin(kx) \sin(lx) \sin(mx) \sin(nx) \times \sin(px) \sin(qx) dx.$$

Equation (32) can be simplified by the transformation

$$c_q = a_q e^{-iq^2 t}$$

yielding

$$i\dot{a}_q + \frac{2}{\pi} \sum_{k,l,m,n,p} a_k a_l a_m a_n^* a_p^* \langle klmpq \rangle \times e^{-i(k^2+l^2+m^2-n^2-p^2-q^2)t} = 0. \quad (33)$$

Similarly, the coupled equations of Fourier amplitudes for the case of septic nonlinearity ($d = 3$) read

$$i\dot{a}_s + \frac{2}{\pi} \sum_{k,l,m,n,p,q,r} a_k a_l a_m a_n^* a_p^* a_q^* a_r^* \langle klmpqr|s \rangle \times e^{-i(k^2+l^2+m^2+n^2-p^2-q^2-r^2-s^2)t} = 0. \quad (34)$$

Note that in Eqs. (33) and (34) most terms are rapidly rotating and average out to zero. Only the ones such that $k^2 + l^2 + m^2 - n^2 - p^2 - q^2 = 0$ for (33) [$k^2 + l^2 + m^2 + n^2 - p^2 - q^2 - r^2 - s^2 = 0$ for (34)] i.e., the resonant terms, will contribute to the long-term dynamics of a_q .

A detailed study can be carried out of the dynamics of the Fourier coefficients for different types of nonlinearities. We have used the Maple software [12] to identify all the resonant terms in the equations for the mode amplitudes. For the cubic nonlinearity ($d = 1$) the amplitude equation equivalent to (33) reads

$$i\dot{a}_j + \frac{2}{\pi} \sum_{k,l,m} a_k a_l a_m^* \langle klm|j \rangle e^{-i(k^2+l^2-m^2-j^2)t} = 0. \quad (35)$$

Taking into account the resonance condition, Eq. (35) turns into the following equations:

$$i\dot{a}_j + a_j \left(\mathcal{P} - \frac{|a_j|^2}{4} \right) = 0, \quad (j = 1, 2, \dots, \infty), \quad (36)$$

where $\mathcal{P} = \sum_{j=1}^{\infty} |a_j|^2$ is conserved. An obvious implication is that $d/dt(|a_j|^2) = 0$ so there is no transfer of energy from one mode to another. Equation (36) admits the solution

$$a_j = |a_j| e^{i(\mathcal{P}-|a_j|^2/4)t}. \quad (37)$$

This analysis is in agreement with the numerical results of Fig. 3. Over a short time the modes oscillate in a periodic fashion; however, their average over a long time is constant. Therefore, for cubic nonlinearity, near $k = 0$, Fourier modes are not coupled in a resonant way. A similar conclusion was reached in Ref. [8] but for a pulselike initial condition. As expected, no collapse will occur in the cubic NLS equation irrespective of the initial total power.

The case of the quintic nonlinearity, ($d = 2$) is more complicated. For simplicity, we consider a solution consisting of three modes, i.e., $m = 1, 3$, and 5 ,

$$\psi(t, x) = a_1 e^{-it} \cos(x) + a_3 e^{-i9t} \cos(3x) + a_5 e^{-i25t} \cos(5x). \quad (38)$$

Equation (33) then gives rise to the following coupled resonant amplitude equations

$$i\dot{a}_1 + a_1 \left[\frac{9}{4} |a_1|^2 \mathcal{P} - \frac{13}{8} |a_1|^4 + 3 |a_3|^2 |a_5|^2 + \frac{9}{8} (|a_3|^4 + |a_5|^4) \right] - \frac{3}{8} a_1^* a_3^3 a_5^* = 0, \quad (39a)$$

$$i\dot{a}_3 + a_3 \left[\frac{9}{4} |a_3|^2 \mathcal{P} - \frac{13}{8} |a_3|^4 + 3 |a_1|^2 |a_5|^2 + \frac{9}{8} (|a_1|^4 + |a_5|^4) \right] - \frac{9}{16} a_1^2 a_3^* a_5^2 = 0, \quad (39b)$$

$$i\dot{a}_5 + a_5 \left[\frac{9}{4} |a_5|^2 \mathcal{P} - \frac{13}{8} |a_5|^4 + 3 |a_1|^2 |a_3|^2 + \frac{9}{8} (|a_1|^4 + |a_3|^4) \right] - \frac{3}{16} a_1^* a_3^2 a_5^3 = 0, \quad (39c)$$

where $\mathcal{P} = |a_1|^2 + |a_3|^2 + |a_5|^2$. It is easy to check that Eqs. (39) satisfy the condition $\frac{d}{dt}(|a_1|^2 + |a_3|^2 + |a_5|^2) = 0$, i.e., \mathcal{P} is a conserved quantity. The last terms in the equations represent the mixing between the three modes and therefore the intensity of each mode is not conserved as in the case of $d = 1$. At this point, note that, if we had included a_7 in

the description, we would have had the additional resonant terms

$$|a_3|^2 a_5^2 a_7, a_5^2 |a_7|^2 a_7^*, a_5^2 |a_5|^2 a_7^*.$$

If $|a_7| \ll 1$, then their contribution would be very small. Another point is that, if we had included the even modes in the description, we would have obtained the extra resonant term $a_2^2 a_4^* a_5$ in the equation for a_1 . This indicates that the modes 2 and 4 couple through mode 5.

Equations (39) can be written into a more compact form by defining $I_j = |a_j|^2$ ($j = 1, 3, 5$). Here, I_j represent the intensity of each mode satisfying $\mathcal{P} = I_1 + I_3 + I_5$. We then obtain

$$\dot{I}_1 = \frac{3}{4} I_1 I_3^{3/2} I_5^{1/2} \sin \theta, \quad (40a)$$

$$\dot{I}_3 = -\frac{9}{8} I_1 I_3^{3/2} I_5^{1/2} \sin \theta, \quad (40b)$$

$$\dot{I}_5 = \frac{3}{8} I_1 I_3^{3/2} I_5^{1/2} \sin \theta, \quad (40c)$$

where $\theta = -2\theta_1 + 3\theta_3 - \theta_5$ with $\theta_j = \arg a_j$. We note that the driving terms on the right-hand side of Eqs. (40) are proportional to the intensities of the modes and their phases. In addition, we have the constraints

$$\frac{4}{3} I_1 + \frac{8}{9} I_3 = \mu_1, \quad (41a)$$

$$\frac{8}{9} I_3 + \frac{8}{3} I_5 = \mu_2, \quad (41b)$$

$$\frac{4}{3} I_1 - \frac{8}{3} I_5 = \mu_1 - \mu_2 = \mu_3, \quad (41c)$$

where μ_i , ($i = 1 - 3$) are constants of the motion. Using the above relations, the dynamics can be reduced to the equations for I_1 and θ . They are

$$\dot{I}_1 = \frac{3}{4} I_1 I_3^{3/2} I_5^{1/2} \sin \theta, \quad (42a)$$

$$\dot{\theta} = \frac{1}{4} (13I_1^2 + 3I_3^2 + 7I_5^2 + 21I_1 I_3 + 27I_1 I_5 + 12I_3 I_5) + \frac{\cos \theta}{8} [6I_1^{1/2} I_3^{3/2} I_5^{1/2} - 27I_1 I_3 I_5^{1/2} - 3I_1 I_3^{3/2} I_5^{-1/2}], \quad (42b)$$

together with the constraints (41).

In order to check the equations for the resonant Fourier modes, we compare the solutions of the reduced equations and the NLS. In Fig. 7 we show the time evolution of the solutions of Eqs. (40) and (1) by using the Runge-Kutta method and split-step Fourier method, respectively. The initial conditions are the same. As expected the amplitudes of the Fourier modes for (1) present fast periodic oscillations. However, over a long time interval the solutions of the reduced equations and the full partial differential equation match well, supporting the validity of the reduced model.

At this point, consider the Neumann boundary conditions for which there is the additional zero mode. This mode leads to the well-known modulational instability. For the cubic nonlinearity $d = 1$, the evolution of the Fourier modes follows (36) so there is no resonant energy exchange between the modes, $\dot{I}_j = 0, j = 0, 1, \dots$. For the quintic nonlinearity $d = 2$, assuming a solution containing the three modes $i = 1, 3, 5$, we obtain evolution equations identical to (39) except that the signs of the resonant terms are reversed. We then obtain the

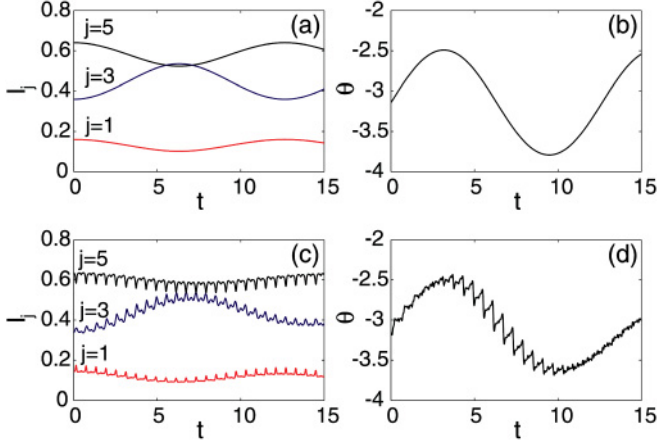


FIG. 7. (Color online) Comparison between the solution of the reduced model and the numerical solution of the NLS for quintic nonlinearity and Dirichlet boundary condition. Panel (a) [respectively, (b)] shows the time evolution $I_1(t)$, $I_3(t)$, and $I_5(t)$ [respectively, the time evolution of $\theta(t)$] for the reduced model (V). Panels (c) and (d) shows the corresponding plots for the partial differential equation. The initial conditions are taken as $I_1 = 0.64$, $I_3 = 0.36$, and $I_5 = 0.16$ and $\theta = -\pi$.

same final equations (42) except that the evolution of the phase θ is reversed.

To show the importance of the zero mode, consider the following example. Assume a solution containing the three first modes $i = 0, 1, 2$, we obtain evolution equations of the form (39) but with no terms outside the brackets. This means that, again, no resonant transfer of energy exists between modes. If the third mode is added to the expansion, new terms appear outside the brackets. The evolution equations are

$$i\dot{a}_0 + a_0[\dots] + \frac{3}{4}a_0^*a_1a_2^*a_3^* = 0, \quad (43a)$$

$$i\dot{a}_1 + a_1[\dots] + \frac{3}{4}a_0^2a_2^*a_3 = 0, \quad (43b)$$

$$i\dot{a}_2 + a_2[\dots] + \frac{3}{2}a_0^2a_1^*a_2^*a_3 = 0, \quad (43c)$$

$$i\dot{a}_3 + a_3[\dots] + \frac{3}{4}a_0^*a_1^2a_2^2 = 0, \quad (43d)$$

where the \dots terms in the brackets are all real. Following a similar procedure as above, the modal energies $I_j = |a_j|^2$ evolve as

$$\dot{I}_0 = \frac{3}{2}I_0I_1^{1/2}I_2I_3^{1/2}\sin\theta, \quad (44a)$$

$$\dot{I}_1 = \frac{3}{2}I_0I_1^{1/2}I_2I_3^{1/2}\sin\theta, \quad (44b)$$

$$\dot{I}_2 = 3I_0I_1^{1/2}I_2I_3^{1/2}\sin\theta, \quad (44c)$$

$$\dot{I}_3 = \frac{3}{2}I_0I_1^{1/2}I_2I_3^{1/2}\sin\theta, \quad (44d)$$

where $\theta = -2\theta_0 + \theta_1 + 2\theta_2 - \theta_3$. As above, one can then reduce the problem to two equations, one for I_0 and one for θ . We do not write these equations because they are cumbersome. The interesting fact is that one needs the 4 modes 0–3 present in order to see this resonant transfer of energy. If one of them is missing, there is no energy transfer. This particular feature of Neumann boundary conditions changes the route for collapse for the Dirichlet case and the Neumann case.

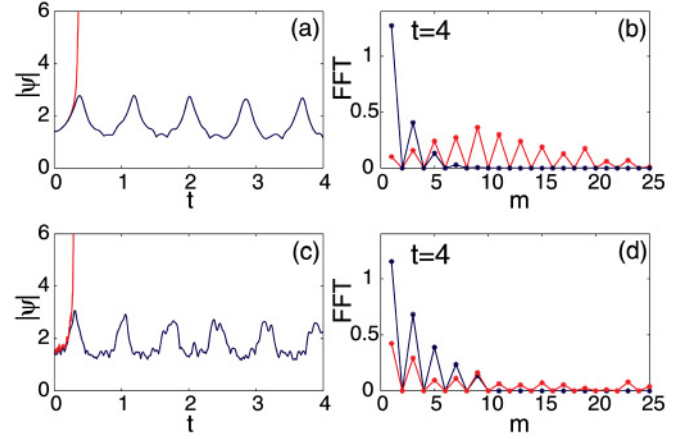


FIG. 8. (Color online) [(a) and (c)] Time evolution of the maximum of $|\psi|$ for quintic nonlinearity with different initial conditions. [(b) and (d)] The corresponding Fourier spectra at $t = 4$. The initial conditions are $\psi(0, x) = 1.4 \sin(x)$ [$P(0) = 3.08$] in (a) and (b), and $\psi(0, x) = 1.4 \operatorname{sech}(x - \frac{\pi}{2})$ [$P(0) = 3.56$] in (c) and (d). We compare the results with and without filtering the high Fourier modes designated, respectively, by the continuous and dashed lines (black and red online). The collapse is efficiently prevented by filtering in both cases.

VI. DISCUSSION AND CONCLUSION

A first outcome of this study is that filtering Fourier modes prevents collapse. This is because the projection of the nonlinear Schrödinger equation on a finite number of Fourier modes yields amplitude equations that are well behaved and do not exhibit collapse. As we have seen, collapse is related to a sudden energy flow to high frequencies. Thus, one can arrest the collapse by filtering the high Fourier modes and, therefore, preventing the sudden energy flow to high frequencies. Physically this can be done by introducing a nonlocal absorption in the model (1). This conclusion is also available for the models with septic nonlinearity and Neumann boundary condition.

In Fig. 8 we show the time evolution of solution with or without filtering high Fourier modes. The initial conditions are taken as a sine wave (the first row) and a hyperbolic secant pulse (the second row). In both cases, the collapse is efficiently prevented by filtering. Because of the absorption of the higher modes, there is a small loss (less than 10%) of the total power. This can be decreased by including more lower frequency modes.

More generally, the resonant transfer amplitude equations can be found in different situations. A first example is the defocusing case. Other types of operators and general boundary conditions can also be studied. As an example consider the following inhomogeneous NLS

$$i\psi_t + d(x)\psi_{xx} + g(x)|\psi|^{2d}\psi = 0, \quad (45)$$

with inhomogeneous Neumann boundary conditions

$$\psi_x(x=0) = a, \psi_x(x=\pi) = b. \quad (46)$$

Then one can transform (45) by setting

$$\phi = \psi - \alpha x(x - \pi) + \beta x \equiv \psi - f(x), \quad (47)$$

where

$$\alpha = \frac{b-a}{2\pi}, \quad \beta = -\frac{a+b}{2}.$$

We obtain

$$i\phi_t + d(x)(\phi_{xx} + \alpha) + g(x)|\phi + f|^{2d}(\phi + f) = 0, \quad (48)$$

with homogeneous Neumann boundary conditions. One can then apply to this equation the formalism we introduced. Of course, the results will not be as simple as for the standard NLS because of the different inhomogeneous terms.

To conclude, we have analyzed and solved numerically the one-dimensional nonlinear Schrödinger equation on a finite interval with Dirichlet or Neumann boundary conditions. A preliminary analysis reveals that $H < 0$ is sufficient for collapse in the Dirichlet case but not for the Neumann case. The bound states have been computed. The first nontrivial one corresponding in the linear limit to $\sin x$ ($\cos x$) for Dirichlet (Neumann) boundary conditions is always linearly stable as opposed to the higher-order modes whose window of stability is very small and reduces as the order is increased.

We have solved the partial differential equation for the cubic and quintic nonlinearities. In the cubic case there is no resonant transfer of energy between Fourier modes, while it is present in the quintic case. Identifying resonant terms in the evolution equations of the Fourier modes, we have written reduced systems. Their evolution is in excellent agreement with the solutions of the NLS, even close to collapse. For the Neumann boundary conditions the Goldstone mode plays a particular role as it couples the modes $m = 1, 2, 3$. For the Dirichlet case, there is no coupling between the first three modes. Note that this model reduction can be extended to higher dimensions and other systems like a cylindrical waveguide. The machinery would be more complicated but the overall method remains the same.

ACKNOWLEDGMENTS

The research of J.G.C. and C.H. was supported by a joint France-Portugal Pessoa agreement. The research of C.H. was supported by the Fundação para a Ciência e a Tecnologia (FCT) under Grant No. SFRH/BPD/36385/2007 and Estímulo à Investigação 2009 de Fundação Calouste Gulbenkian. The authors thank Vladimir Konotop for very helpful discussions.

APPENDIX A: NUMERICAL PROCEDURE FOR SOLVING THE 1D NLS (1)

The 1D nonlinear Schrödinger equation (1) with Dirichlet or Neumann boundary conditions is solved as usual by splitting the linear and nonlinear part of the operator. The linear part

$$iu_t + u_{xx} = 0, \quad (A1)$$

is such that

$$\hat{u}(dt) = e^{-ik^2 dt} \hat{u}(0),$$

where \hat{u} is the sine or cosine Fourier transform of u to satisfy the boundary conditions. The solution of the nonlinear stepping is the standard one

$$u(2dt) = e^{i|u(dt)|^{2d} dt} u(dt).$$

The numerical implementation is done in MATLAB [13] and the solution is evaluated at discrete points $u_n, n = 1, \dots, N$. The sine and cosine Fourier transforms for the linear step (A1) are then done using the discrete sine and cosine Fourier transforms.

For the Dirichlet boundary conditions, we use the discrete sine Fourier transform

$$\hat{u}(k) = \sum_{n=1}^N u(n) \sin\left(\frac{\pi kn}{N+1}\right), \quad k = 1, \dots, N, \quad (A2)$$

and inverse discrete sine Fourier transform

$$u(n) = \sum_{k=1}^N \hat{u}(k) \sin\left(\frac{\pi kn}{N+1}\right), \quad n = 1, \dots, N. \quad (A3)$$

The Neumann boundary conditions are trickier to implement because one needs to use the discrete cosine Fourier transform

$$\hat{u}(k) = w(k) \sum_{n=1}^N u(n) \cos\left[\frac{\pi(2n-1)(k-1)}{2N}\right], \quad k = 1, \dots, N, \quad (A4)$$

with

$$w(1) = 1/\sqrt{N}, \quad w(k) = \sqrt{\frac{2}{N}}, \quad 2 \leq k \leq N.$$

The inverse discrete cosine Fourier transform is

$$u(n) = \sum_{k=1}^N w(k) \hat{u}(k) \cos\left[\frac{\pi(2n-1)(k-1)}{2N}\right], \quad n = 1, \dots, N. \quad (A5)$$

The number of discretization points was chosen to be $N = 2^{11} - 1$ or $N = 2^{12} - 1$ with a step $dt = 10^{-4}$. The L_2 norm was checked during the computation and it is conserved up to 10^{-10} in absolute value.

APPENDIX B: PARITY ARGUMENT FOR THE MODE CASCADE

In order to prove Eq. (28), consider the case of $d = 1$ and Neumann boundary conditions. The argument for the cases $d = 2, 3$ are similar. Equation (1) with $d = 1$ can be written into the form

$$\psi(t+dt, x) = \psi(t, x) + i \left[\frac{1}{2} \frac{\partial^2 \psi(t, x)}{\partial x^2} + |\psi(t, x)|^2 \psi(t, x) \right] dt, \quad (B1)$$

for small dt . We now assume that the initial condition is taken as $\psi(0, x) = \cos(qx) = \frac{1}{2}(e^{iqx} + e^{-iqx})$. Substituting the initial condition into Eq. (B1), we have

$$\psi(dt, x) = \frac{1}{2}(e^{iqx} + e^{-iqx}) + i \left[-\frac{1}{4}(e^{iqx} + e^{-iqx}) + \frac{1}{8}(e^{3iqx} + 3e^{iqx} + 3e^{-iqx} + e^{-3iqx}) \right] dt. \quad (B2)$$

As we see, after a short time interval dt , the solution $\psi(dt, x)$ can be expressed as $\psi(dt, x) = c_q \cos(qx) + c_{3q} \cos(3qx)$. We can repeat this process and obtain that $\psi(t, x) = \sum_{m=(2n-1)q} c_m \cos(mx)$ ($n = 1, 2, \dots$). In other words for $d = 1$ we obtain modes 1, 3, and 5 while for $d = 2$ we obtain modes 1, 3, 5, and 7, and so on. This simple argument, using as time integrator an explicit Euler scheme, can be extended to other time integrators.

Note that, if we had introduced a symmetry breaking in the operator, for example, by multiplying the dispersion or nonlinearity by a function of x , then we would get both odd and even modes for a $\cos(qx)$ initial condition. Also note that the zero mode $m = 0$ does not give rise to any cascade to higher Fourier modes.

APPENDIX C: EVOLUTION OF THE RESONANT FOURIER MODES FOR THE NEUMANN BOUNDARY CONDITIONS

For the Neumann case, we expand ψ in a cosine Fourier series

$$\psi(x, t) = \sum_{m=0}^{\infty} c_m(t) \cos(mx), \quad (\text{C1})$$

where the c_m are given by

$$c_0(t) = \frac{1}{\pi} \int_0^\pi \psi(x, t) dx, \quad (\text{C2a})$$

$$c_n(t) = \frac{2}{\pi} \int_0^\pi \psi(x, t) \cos(nx) dx \quad (n \neq 0). \quad (\text{C2b})$$

Substituting the expansion (C1) into Eq. (1), we obtain the coupled equations of Fourier amplitudes for the case of quintic nonlinearity ($d = 2$)

$$i\dot{c}_0 + \frac{1}{\pi} \sum_{k,l,m,n,p} c_k c_l c_m c_n^* c_p^* \langle klmp|0 \rangle = 0, \quad (\text{C3a})$$

$$i\dot{c}_q - q^2 c_q + \frac{2}{\pi} \sum_{k,l,m,n,p} c_k c_l c_m c_n^* c_p^* \langle klmp|q \rangle = 0, \quad (\text{C3b})$$

$(q \neq 0),$

where

$$\langle klmp|q \rangle \equiv \int_0^\pi \cos(kx) \cos(lx) \cos(mx) \cos(nx) \times \cos(px) \cos(qx) dx.$$

Equations (C3) can be simplified by the transformation

$c_q = a_q e^{-iq^2 t}$ to yield

$$i\dot{a}_q + \frac{\sigma_q}{\pi} \sum_{k,l,m,n,p} a_k a_l a_m a_n^* a_p^* \langle klmp|q \rangle \times e^{-i(k^2+l^2+m^2+n^2-p^2-q^2)t} = 0, \quad (\text{C4})$$

where $\sigma_q = 1$ for $q = 0$ and $\sigma_q = 2$ for $q \neq 0$. Similarly, the coupled equations of Fourier amplitudes for the case of septic nonlinearity ($d = 3$) read

$$i\dot{a}_s + \frac{\sigma_s}{\pi} \sum_{k,l,m,n,p,q} a_k a_l a_m a_n a_p^* a_q^* a_r^* \langle klmpqr|s \rangle \times e^{-i\frac{1}{2}(k^2+l^2+m^2+n^2-p^2-q^2-r^2-s^2)t} = 0, \quad (\text{C5})$$

where $\sigma_s = 1$ for $s = 0$ and $\sigma_s = 2$ for $s \neq 0$.

For simplicity, we consider the solution (38). Then, Eq. (C4) turns into the following coupled equations:

$$i\dot{a}_1 + a_1 \left[\frac{9}{4} |a_1|^2 \mathcal{P} - \frac{13}{8} |a_1|^4 + 3 |a_3|^2 |a_5|^2 + \frac{9}{8} (|a_3|^4 + |a_5|^4) \right] + \frac{3}{8} a_1^3 a_3^2 a_5^* = 0, \quad (\text{C6a})$$

$$i\dot{a}_3 + a_3 \left[\frac{9}{4} |a_3|^2 \mathcal{P} - \frac{13}{8} |a_3|^4 + 3 |a_1|^2 |a_5|^2 + \frac{9}{8} (|a_1|^4 + |a_5|^4) \right] + \frac{9}{16} a_1^2 a_3^* a_5 = 0, \quad (\text{C6b})$$

$$i\dot{a}_5 + a_5 \left[\frac{9}{4} |a_5|^2 \mathcal{P} - \frac{13}{8} |a_5|^4 + 3 |a_1|^2 |a_3|^2 + \frac{9}{8} (|a_1|^4 + |a_3|^4) \right] + \frac{3}{16} a_1^* a_3^3 = 0, \quad (\text{C6c})$$

where $\mathcal{P} = |a_1|^2 + |a_3|^2 + |a_5|^2$. These are exactly the same as (39) except that the terms outside the brackets have the opposite signs.

As done above, Eqs. (C6) can be written into a more compact form by defining $I_j = |a_j|^2$ ($j = 1, 3, 5$), i.e.,

$$\dot{I}_1 = -\frac{3}{4} I_1 I_3^{3/2} I_5^{1/2} \sin \theta, \quad (\text{C7a})$$

$$\dot{I}_3 = \frac{9}{8} I_1 I_3^{3/2} I_5^{1/2} \sin \theta, \quad (\text{C7b})$$

$$\dot{I}_5 = -\frac{3}{8} I_1 I_3^{3/2} I_5^{1/2} \sin \theta, \quad (\text{C7c})$$

where $\theta = -2\theta_1 + 3\theta_3 - \theta_5$ with $\theta_j = \arg a_j$. Equation (C7) can be further written into the form

$$\dot{I}_1 = -\frac{3}{4} I_1 I_3^{3/2} I_5^{1/2} \sin \theta, \quad (\text{C8a})$$

$$\dot{\theta} = \frac{1}{4} (13I_1^2 + 3I_3^2 + 7I_5^2 + 21I_1 I_3 + 27I_1 I_5 + 12I_3 I_5) - \frac{\cos \theta}{8} [6I_1^{1/2} I_3^{3/2} I_5^{1/2} - 27I_1 I_3 I_5^{1/2} - 3I_1 I_3^{3/2} I_5^{-1/2}], \quad (\text{C8b})$$

together with the constraints (41).

[1] L. Bergé, *Phys. Rep.* **303**, 259 (1998).

[2] C. Sulem and P.-L. Sulem, *The Nonlinear Schrödinger Equation* (Springer, New York, 1999).

[3] H. Brezis and T. Gallouet, *Nonlinear Analysis* **4**, 677 (1980).

[4] W. Strauss and C. Bu, *J. Differ. Equations* **173**, 79 (2001).

[5] G. Fibich and F. Merle, *Physica D* **155**, 132 (2001).

[6] J. G. Caputo and M. P. Soerensen, *Eur. Phys. J. Special Topics* **147**, 265 (2007).

- [7] J. I. Ramos and F. R. Villatoro, *Math. Comput. Model.* **20**, 31 (1994).
- [8] M. B. Erdogan and V. Zharnitsky, *Commun. Math. Phys.* **281**, 655 (2008).
- [9] D. J. Muraki, *SIAM J. Appl. Math.* **67**, 1504 (2007).
- [10] V. Zakharov, F. Dias, and A. Pushkarev, *Phys. Rep.* **398**, 1 (2004).
- [11] H. S. Carslaw, *Introduction to the Theory of Fourier Series and Integrals* (Dover, London, 1980).
- [12] Maple software [<http://www.maplesoft.com/>].
- [13] The MathWorks [<http://www.mathworks.com/>].